

# Effect of manganese on the texture of twin-roll cast AlMg3 sheets

M. Slámová<sup>1\*</sup>, P. Sláma<sup>1</sup>, M. Janeček<sup>2</sup>, Y. Birol<sup>3</sup>

<sup>1</sup>Research Institute for Metals, Panenské Břežany 50, 250 70 Odolena Voda, Czech Republic

<sup>2</sup>Charles University, Faculty of Mathematics and Physics, Ke Karlovu 5, 121 16 Prague 2, Czech Republic

<sup>3</sup>Materials Institute, Marmara Research Center, Tubitak, Gebze, Kocaeli, Turkey

Received 19 February 2008, received in revised form 13 March 2008, accepted 4 April 2008

## Abstract

The use of aluminium alloy sheets in cars allows improving fuel economy and reducing emissions. Sheet manufacturing based on twin-roll casting (TRC) is a cost effective technology that is a promising candidate for replacing the actual direct-chill casting technology. The effect of Mn content and pre-treatment on the grain structure and texture of recrystallized sheets produced from TRC AlMg3 alloys was investigated. Grain size and uniformity are affected mostly by the degree of deformation prior to annealing. The effect of Mn supersaturation and precipitation concurrent with recrystallization on grain size is less pronounced but both significantly reduce texture strength, especially this of the cube component. The mechanisms of the effect of Mn on texture were elucidated. High Mn solute supersaturation ensures suppression of cube texture development and prevents sheet anisotropy in forming procedures.

**Key words:** aluminium-magnesium alloys, manganese, twin-roll casting, grains, texture

## 1. Introduction

The use of aluminium and magnesium alloys in the automotive industry is nowadays a well-established practice, which enables to improve vehicle fuel economy and reduce emissions [1]. The advantage of aluminium over steel, its competitor in automotive applications, is the very attractive combination of low density, high strength and formability, the ease of recycling and high corrosion resistance. While Al die-cast parts are extensively used, the use of Al sheet is relatively scarce. The major barrier to the widespread use of Al sheets in automotive applications is the high cost, which is four to five times that of steel sheets. Production of Al sheets by twin-roll continuous (TRC) casting, rather than by the conventional direct-chill casting (DCC) and hot rolling route, offers an opportunity to substantially reduce sheet cost.

Due to their good formability, DCC AA5xxx alloy sheets in the soft condition are often used for manufacturing car-body inner panels or other automotive parts. In spite of their low cost, the TRC sheets have not found widespread use due to their specific micro-

structural features and properties markedly different from those of DCC materials. Due to the high solidification rate intrinsic for TRC casting, aluminium alloys issued from TRC have high supersaturation of alloying elements in solid solution. This often has an unfavourable effect on their response to heat treatments and the resulting structure and properties, especially on their grain structure and formability [2, 3]. Sheet formability is strongly affected by structural anisotropy that is the cause of earing and inhomogeneous distribution of strain through thickness. Earing is minimized in sheets with suitable crystallographic texture. The texture should be either random or a well balanced mixture of components that promote earing at different angles to the rolling direction, i.e., a suitable combination of cube and retained rolling texture [4].

The effect of processing parameters and composition on the formability of DCC AA5xxx alloys has been extensively studied [4–7]. The ductility and bendability of AA5754 automotive sheets have been investigated as a function of iron content in [6], the effect of Mn on the strength and formability of AlMg3

\*Corresponding author: tel./fax: +420 283 971 816; e-mail address: [slamova@vzskum-kovu.cz](mailto:slamova@vzskum-kovu.cz)

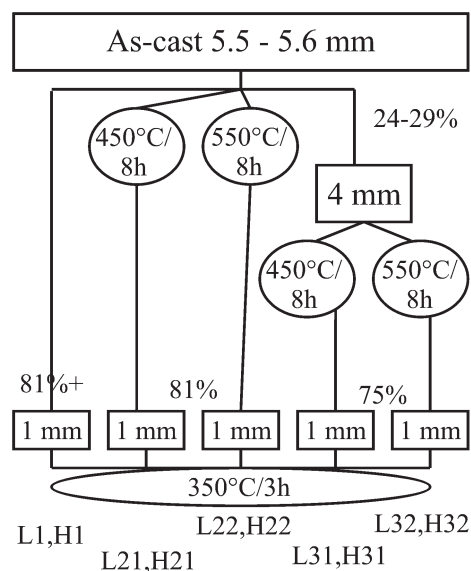


Fig. 1. Schematics of the processing routes used in the experiment.  $Lxy$  are low-Mn specimens,  $Hxy$  are specimens with 0.22 wt.% Mn ( $x = 1, 2, 3; y = 1, 2$ ).

alloys was studied in [7]. The properties of magnesium alloys are extensively presented in [8]. Morris et al. have carried out extensive studies of belt-cast AA5xxx strips, especially of the textures developing in these materials [9, 10]. On the other hand, the knowledge of the microstructure (including texture) and the related properties of TRC Al-Mg sheets is still very scarce.

Our previous investigations [11, 12] have indicated that the microstructure, texture and properties of TRC Al-Mg alloys are significantly affected not only by down-stream processing parameters but also by the content of minor alloying elements such as manganese and chromium. The objective of the present paper is to evaluate and elucidate in more detail the effect of Mn on the microstructure and texture of TRC AlMg3 (AA5754) sheets. Two sets of specimens differing in Mn content were processed by schemes simulating real industrial technologies (Fig. 1). Specimen microstructure, texture and properties were evaluated. Microstructure and mechanical properties are reported in [12], the present paper focuses on the effect of Mn on grain structure and texture. The mechanisms of this effect, especially the impact of Mn precipitation on the recrystallization and the resulting texture, are discussed.

## 2. Experimental

TRC strips of the commercial alloy AA5754 differing in Mn and Mg contents (Table 1) were investigated. The input materials were sheets of thickness of 5.2 mm and 5.6 mm. Sheets of 1.0 mm thickness

Table 1. Chemical composition of the alloys (in wt.%)

Element	Mg	Mn	Fe	Si	Cu
High Mn, Mg	3.07	0.22	0.29	0.12	0.03
Low Mn, Mg	2.68	0.04	0.27	0.12	0.01

in the soft temper were prepared using five different schemes of thermo-mechanical treatment (Fig. 1). One set of specimens was processed without homogenization, i.e., the specimens were cold rolled from the as-cast sheets directly to the final thickness. The other processing cycles involved industrial-like homogenization consisting of slow heating, followed by soaking at 450°C and 550°C, respectively, and by slow cooling to room temperature (RT). Homogenization was done either in the as-cast condition or after a slight thickness reduction of 24 or 29%. All 1.0 mm strips were annealed at 350°C for 3 hours. In order to simulate industrial conditions of batch coil annealing, slow heating and slow cooling to RT were used. The specimens of the alloy with high Mn content are referred to as  $Hxy$ , while those with very low Mn content as  $Lxy$  (Fig. 1).

The microstructure and grain structure were investigated by light and transmission electron microscopy (LM and TEM). Second phase particles were observed after etching with a 0.5% HF solution in water. Barker's solution anodising and polarized light microscopy allowed the observation of grain structures. Thin foils for TEM were prepared by electropolishing in a 30% solution of  $\text{HNO}_3$  in methanol at  $-17^\circ\text{C}$  using a twin jet device. TEM observations were performed using a Philips CM 100 operated at the 200 kV. Texture analyses were carried out by standard X-ray diffraction techniques. The data of the (111), (200) and (220) incomplete pole figures were used to compute the three-dimensional orientation distribution functions (ODF) by the series expansion method with expansion to  $l_{\text{max}} = 22$  [13]. The textures were measured at two positions: at sheet surface and at sheet central plane (mid-thickness).

## 3. Results

LM examinations revealed in all specimens fine second-phase particles (Fig. 2), the fraction, size and spatial distributions of which depend on the processing cycle and alloy composition. The fraction of particles is higher in the Mn-rich specimens. Previous LM examinations showed that the specimens with high Mn homogenized at 450°C exhibit a bimodal particle size distribution (Figs. 2c, 3d), i.e., they contain relatively coarse constituent particles and a dense

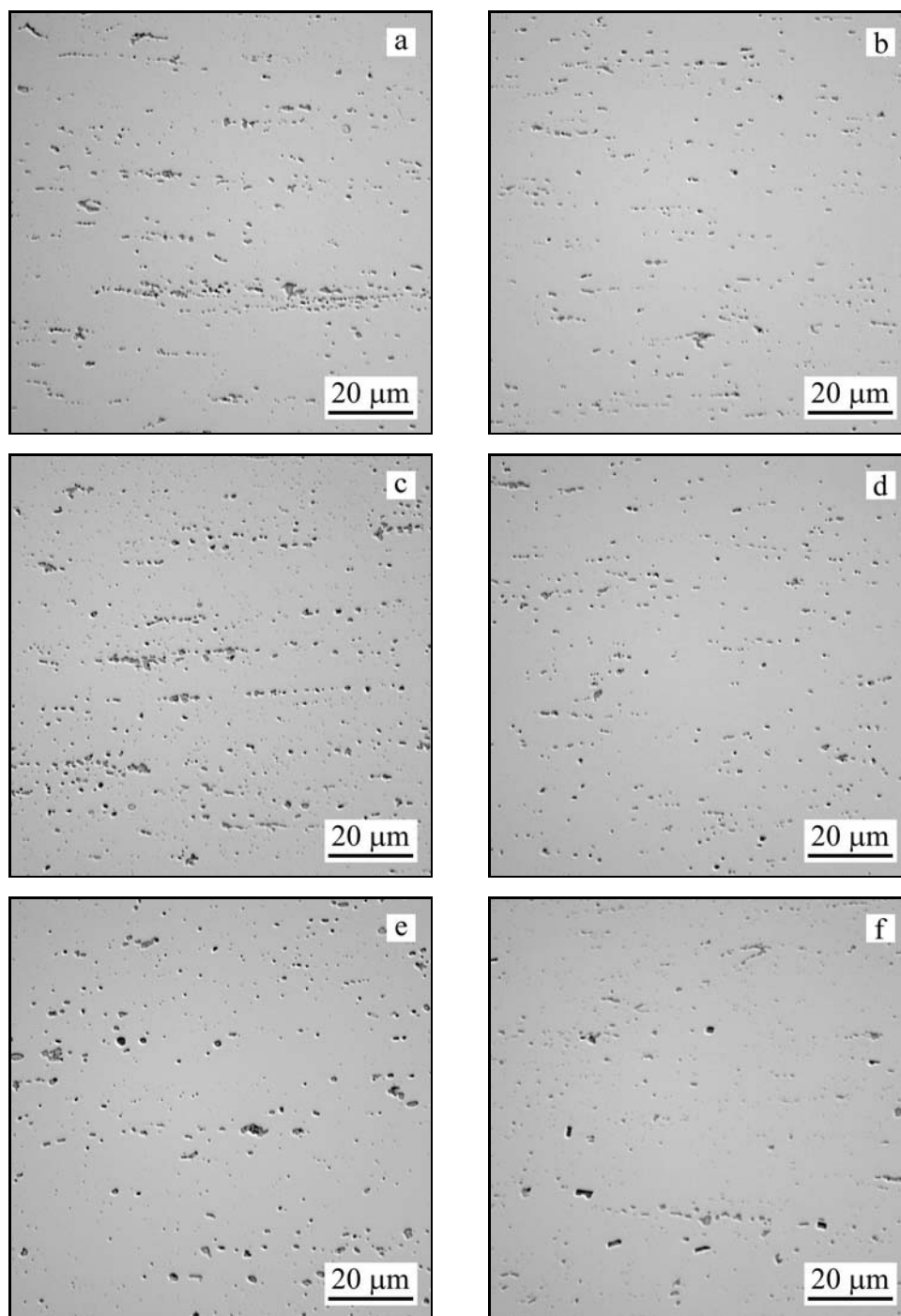


Fig. 2. Micrographs of second-phase particles in specimens (for processing details – see Fig. 1): a) H1; b) L1; c) H21; d) L21; e) H22; f) L22. Specimens with high and low Mn content are in the left-hand and right-hand column, respectively.

population of tiny precipitates. TEM examinations revealed the presence of precipitates also in the other specimens (Fig. 3). The biggest and most evenly distributed constituent particles are observed in specimens H32 and L32, whereas the non-homogenized specimens H1, L1 have finer particles clustered in strings. The constituent particles in the specimens homogenized at 450°C (Fig. 2c,d) are smaller and more numerous as compared to their counterparts homogenized

at 550°C (Fig. 2e,f). The precipitates are coarser in the Mn-rich specimens than in the low-Mn variety (Fig. 3a,c,d and Fig. 3b). These precipitates are the most dense in the non-homogenized specimen (Fig. 3a), the least dense in those homogenized at 450°C (Fig. 3b,d) and are the biggest in those homogenized at 550°C.

Recrystallized structure is observed in all specimens (Fig. 4) but the average grain size is significantly

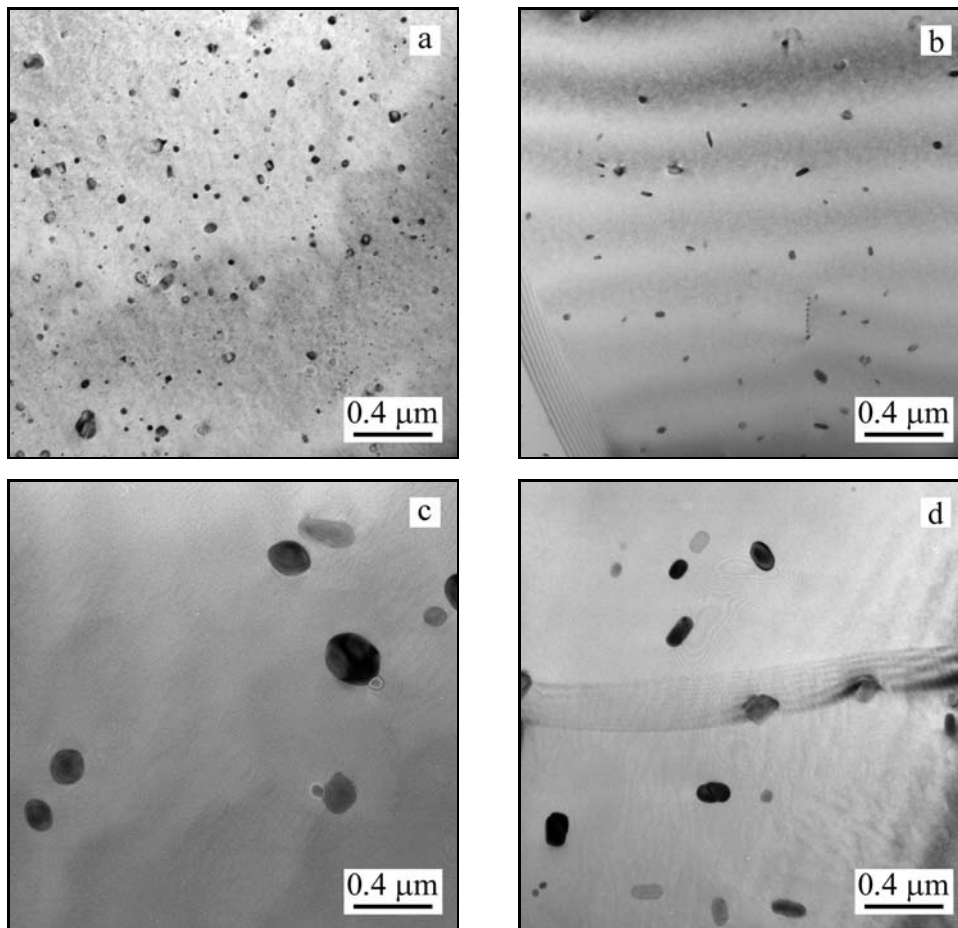


Fig. 3. TEM micrographs showing the dispersoids in specimens (for processing details – see Fig. 1): a) H1; b) L31; c) H32; d) H31.

Table 2. Mean grain size in the rolling and normal directions (RD, ND) of the different pre-treatment variants (in  $\mu\text{m}$ )

Mn content	Variant	1	21	22	31	32
High	RD	12	23	15	16	15
Low		14	24	20	17	17
High	ND	7	12	13	11	10
Low		8	12	16	11	12

different. In some of the specimens, the grains are not uniform in size (Fig. 4c,d). The grains in the high-Mn specimens are finer than in their low-Mn counterparts (Table 2). The mean grain sizes in the rolling direction (RD) of the former are in the range from 12 to 23  $\mu\text{m}$  and from 14 to 24  $\mu\text{m}$  in the latter. The grain sizes in the direction normal to the rolling plane (ND) differ even more: from 7 to 13  $\mu\text{m}$  in the former and from 8 to 16  $\mu\text{m}$  in the latter. The non-homogenized variants H1 and L1 (Fig. 4a,b) reveal the smallest (Table 2) and most uniform grains. Coarser (Table 2) and more uniform grains are observed in the variants homogen-

ized after a cold rolling pass (Fig. 4e,f). Regions with very coarse grains along with clusters of fine grains are present in the sheets homogenized in the as-cast condition (Fig. 4c,d). The temperature of homogenization does not have a prominent effect on grain size and uniformity.

The results of texture measurements are presented in the form of Orientation Distribution Function (ODF) graphs in Figs. 5 and 6 (at mid-thickness and at surface, respectively). Graphs comparing the orientation densities  $f(g)$  measured at mid-thickness along the  $\beta$ -fibre and  $\varphi_1$ -axis ( $\Phi = 0^\circ$ ,  $\varphi_2 = 0^\circ$ ) in the ODF space are shown in Fig. 7. Such a texture representation allows easier estimation of the differences in the strength of texture components, such as cube, cube<sub>RD</sub> and cube<sub>ND</sub> and the components of the  $\beta$ -fibre, i.e., brass (Bs), copper (Cu) and S.

Several general outcomes are evident by comparing the textures of the specimens differing in composition and processing parameters (Figs. 5, 6 and 7):

1. All specimens exhibit textures containing cube orientations and components of the rolling texture, i.e., of the  $\beta$ -fibre. Goss component is present in some specimens.

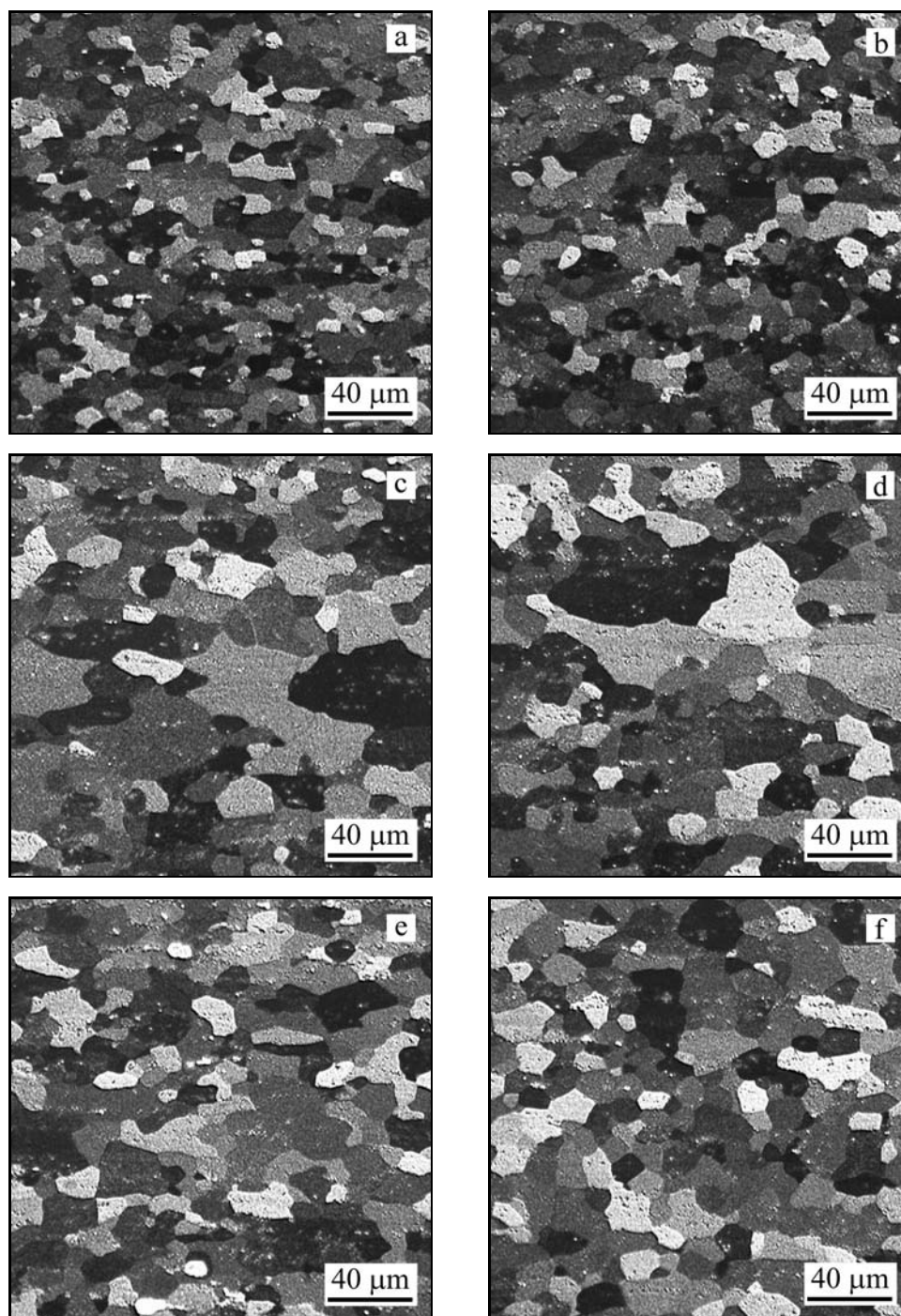


Fig. 4. Micrographs of the grain structure in specimens (for processing details – see Fig. 1): a) H1; b) L1; c) H21; d) L21; e) H31; f) L31. Specimens with high and low Mn content are in the left-hand and right-hand column, respectively.

2. All specimens with low Mn content exhibit stronger texture than their high-Mn counterparts.

3. All specimens with high Mn exhibit similar and weak textures with maxima not exceeding 4-times the strength of random texture, whereas the strength of texture in the low-Mn specimens is up to 12- or 15-times higher than that of the random one.

4. The cube component is much stronger in the low-Mn specimens than in the specimens with high

Mn, especially when homogenized at 450 °C.

5. The strength of the texture at mid-thickness of low-Mn sheets depends on the processing scheme. The strongest texture is observed in the variants homogenized at 450 °C, followed by these with homogenization at 550 °C. The specimens without any homogenization present the weakest texture.

6. Contrarily to the specimens with high Mn content, the textures at the surface of the specimens

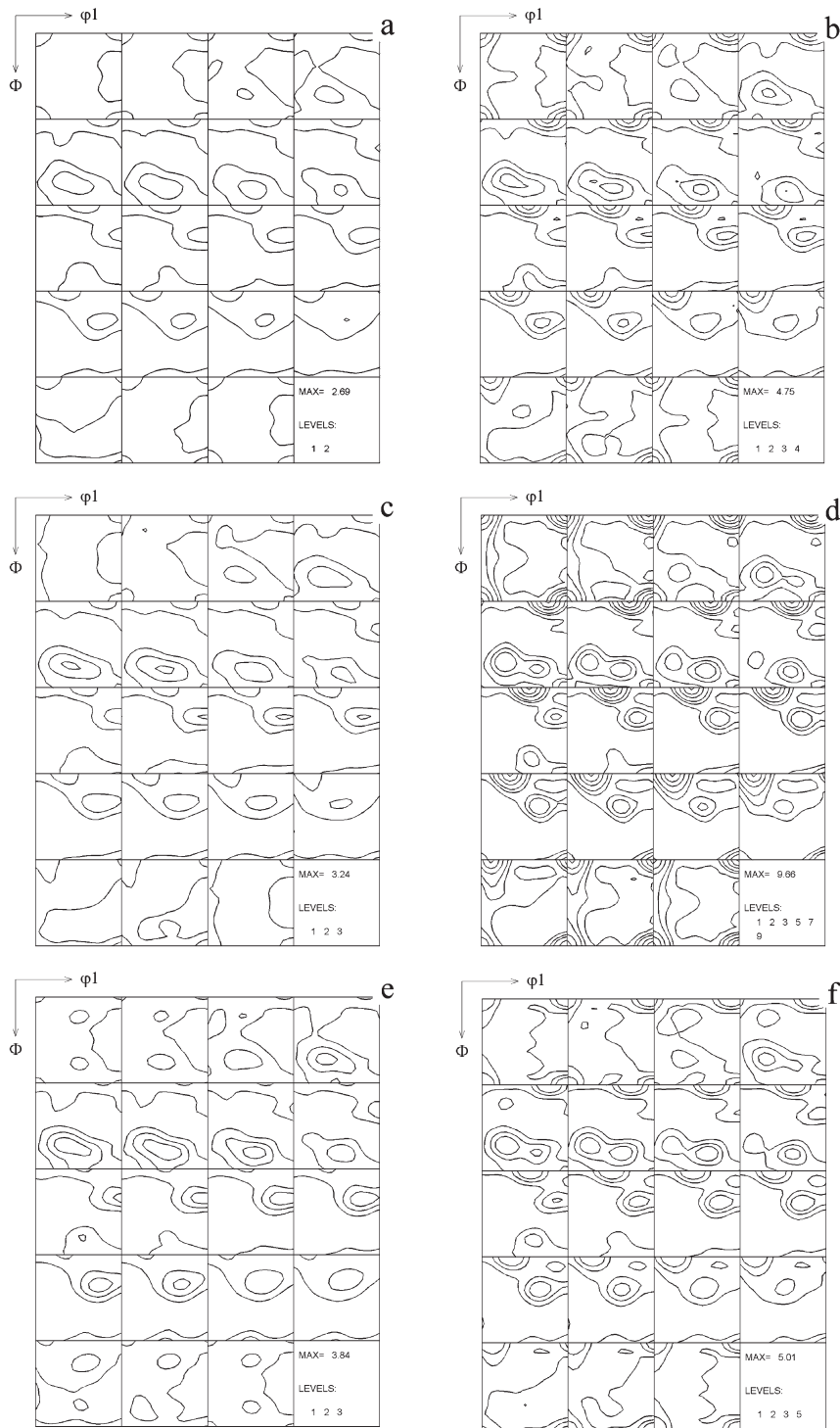


Fig. 5. ODFs at the mid-thickness of specimens (for processing details – see Fig. 1): a) H1; b) L1; c) H21; d) L21; e) H22; f) L22. Specimens with high and low Mn content are in the left-hand and right-hand column, respectively.

with low Mn content are stronger than at their mid-thickness. The most striking example of such a difference is the specimen L1 prepared without homogenization. Specimen L1 has a surface texture with the strongest cube and  $\beta$ -fibre components among all measured specimens but the strength of the texture

at mid-thickness is moderate. The specimens L21 and L31 of the same alloy with low Mn (homogenized at 450 °C) also exhibit strong cube and  $\beta$ -fibre components but the difference between mid-thickness and surface is smaller.

7. Besides the simple cube component, orientations

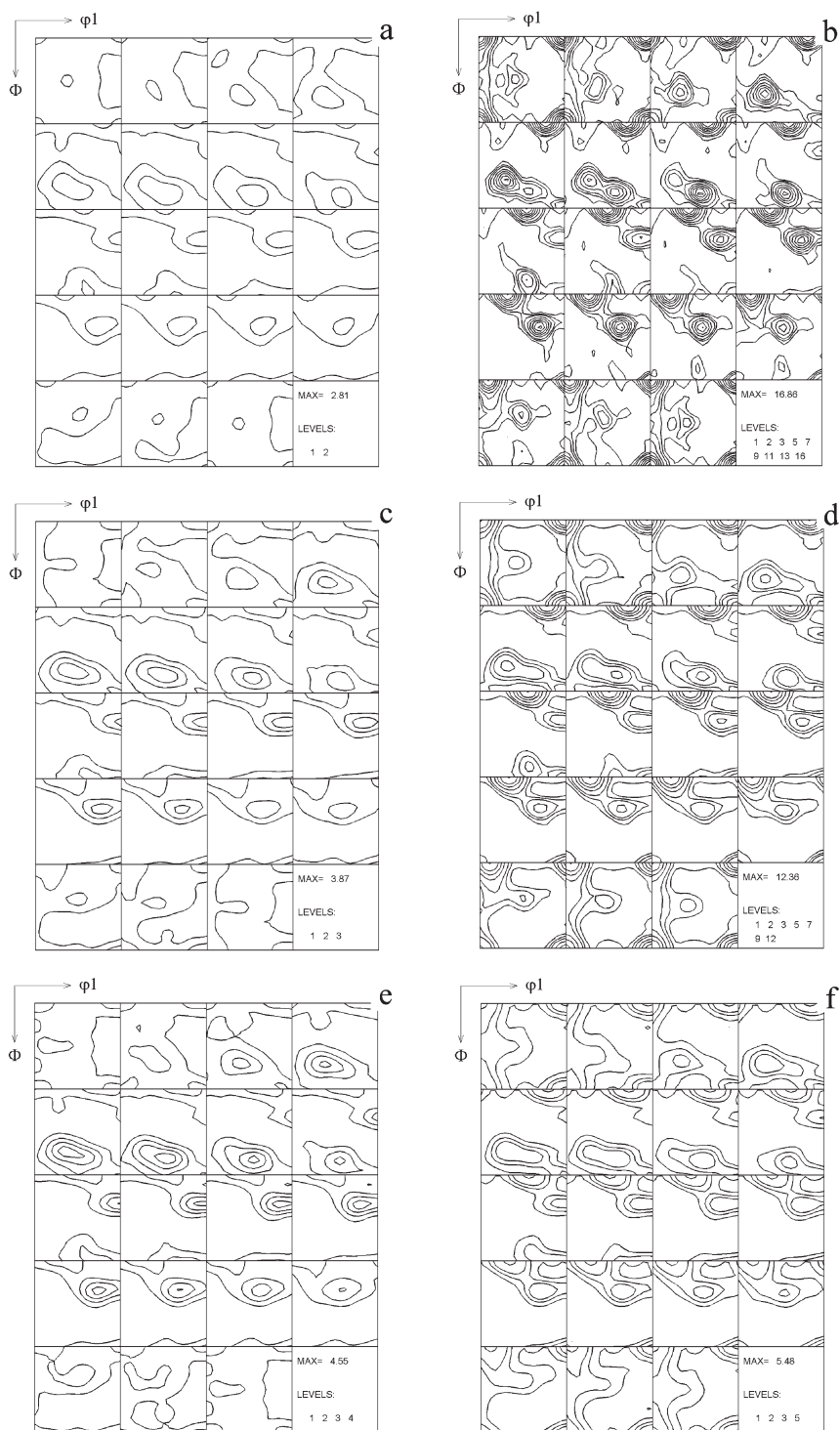


Fig. 6. ODFs at the surface of specimens (for processing details – see Fig. 1): a) H1; b) L1; c) H21; d) L21; e) H22; f) L22. Specimens with high and low Mn content are in the left-hand and right-hand column, respectively.

rotated about the normal sheet direction ( $\text{cube}_{\text{ND}}$  and  $\text{cube}_{\text{shear}}$ ) are relatively strongly represented in the texture of the surface layers of the majority of low-Mn specimens and are weak in the surface texture of the high-Mn specimens.

#### 4. Discussion

##### 4.1. Effect of composition and pre-treatment on phase composition and transformations

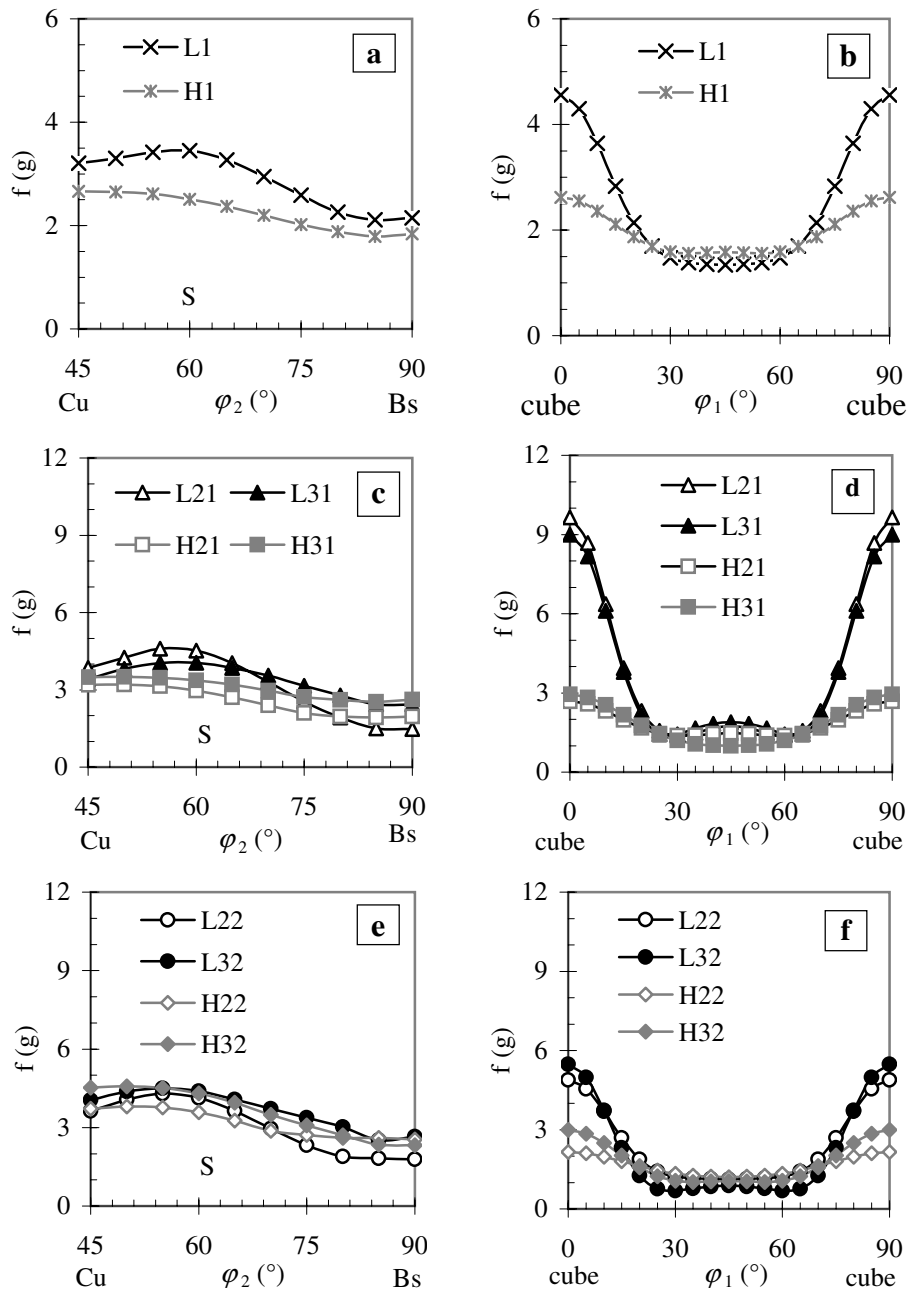


Fig. 7. Orientation densities  $f(g)$  along the  $\beta$ -fibre (a, c, e) and the  $\varphi_1$ -axis (b, d, f) measured at mid-thickness of the specimens without homogenization (a, b) and these homogenized at 450°C (c, d) and 550°C (e, f).

All investigated materials are expected to have high solute supersaturation of Mg before the final annealing. Therefore, Mg precipitation may occur before or simultaneously with recrystallization. In the non-homogenized specimens Mg solute is retained from the as-cast condition and the precipitation process is the most intensive. In the homogenized samples,  $\text{Al}_3\text{Mg}_2$  precipitation may occur during the slow heating but since this phase dissolves above 400°C, it is highly probable that the supersaturation of solute Mg in these specimens is also high. It is well known that the pinning of dislocations by concurrent pre-

cipitation effectively inhibits subgrain growth and thus retards the nucleation stage of the recrystallization. However, analyses of the effectiveness of concurrent precipitation in Al-Mg alloys by Morris and Liu [10] have proved that the  $\text{Al}_3\text{Mg}_2$  precipitates are not effective in hindering recrystallization. Therefore, when an effect of concurrent precipitation on recrystallization is observed in AA5754 alloy, it has to be attributed mainly to the precipitation of Mn or Cr containing particles. During the TRC casting of AA5754 alloys non-equilibrium phases of Al with Fe, Si and Mn form constituent particles but a

large fraction of Mn atoms remains in solid solution [12, 14]. Some  $Mg_2Si$  and  $Al_3Mg_2$  particles are also present. During homogenization, phase transformations take part. Mn together with Si and Fe solutes forms precipitates that grow with increasing temperature during heating or during holding at 450 °C. The same elements participate in the transformation of non-equilibrium constituent particles into equilibrium ones. At high temperatures (550 °C), particle coarsening occurs. Above 450 °C some dissolution of small precipitates occurs and provides Mn, Si and Fe for the progressive coarsening of constituent particles. In high-Mn specimens  $Al_6(Mn,Fe)$  and  $\alpha-Al_{12}(Mn,Fe)_3Si$  precipitates form at temperatures above 250 °C. In alloys with low Mn content  $Al_3Fe$  and  $Al_6Fe$  phases can precipitate but since a considerable amount Si is also present,  $Al_8Fe_2Si$  or Mn-free  $\alpha-AlFeSi$  cubic precipitates are likely to form, too. The Mn-free precipitates are smaller than the precipitates with Mn in the specimens with high content of Mn (Fig. 3).

The supersaturation of solute atoms available for precipitation during the softening annealing of the 1.0 mm sheets depends on sheet pre-treatment. Non-homogenized specimens have the highest solute content, followed by the specimens homogenized at 550 °C and at 450 °C. Homogenization at 450 °C is known to almost completely remove the Mn solute atoms from the matrix.

#### 4.2. Effect of alloy composition and pre-strain on grain size and uniformity

Several factors can affect the grain size of thermally softened materials [15]:

a) *Degree of working (deformation) prior to annealing.* The grain size usually decreases with increasing degree of working. In our case, the deformation is introduced by the cold rolling, and partially also by the hot rolling involved in TRC.

b) *Coarse constituent particles* promote the particle stimulated nucleation (PSN) of new grains. Therefore, the size and uniformity of grains depend on the size and spatial distribution of constituents. PSN, i.e., discontinuous recrystallization, is active at high temperatures. Continuous recrystallization is more probable at low temperatures.

c) *Supersaturation of the matrix.* Solute atoms hinder dislocation motion and thus prevent the dynamic recovery during rolling. Higher solute content results in higher stored energy and acts similarly as the degree of deformation (see a)). However, as solute atoms can precipitate, their effect on grain size is ambiguous.

d) *Precipitation of particles* that are known to nucleate preferentially on dislocations. Precipitates prevent dislocation motion and their polygonization in

low-angle grain boundaries, i.e., the nucleation of subgrains. High solute supersaturation and concurrent precipitation thus can shift both the start and end of recrystallization to higher temperatures during slow heating or retard it when isochronal annealing is employed. The effect of concurrent precipitation depends obviously on the degree of deformation since precipitation is facilitated by a high dislocation density.

The specimens processed without homogenization have significantly smaller grain size than the specimens pre-treated with homogenization. The observed difference is caused by the difference in pre-strain. Furthermore, high angle grain boundaries (HAGB) are preferred nucleation sites for recrystallization in Al-Mg alloys. The non-homogenized specimens exhibit higher fraction of HAGB than their homogenized counterparts that probably plays also some role in the grain refinement.

The dragging force exerted on dislocations and grain boundaries by Mn-bearing precipitates forming concurrently with or before recrystallization is also important. Precipitation is the most intensive in the non-homogenized specimens because they have the highest Mn solute content. In order to be effective, the concurrent precipitation must be thermally stable at the corresponding annealing temperature, the precipitates must be of small size (10 to 100 nm) and of sufficient density to produce a significant pinning effect [10]. The non-homogenized H1 specimen contains after the annealing the most dense and sufficiently fine precipitates (Fig. 3). The precipitates are much less dense in its low-Mn counterpart L1. The larger grain size in specimen L1 evidences the effect of concurrent precipitation on grain size in these specimens. The specimens H22, H32, L22, and L32 (homogenized at 550 °C) contain the biggest and less dense precipitates (Fig. 3) that were formed during the homogenization and obviously were not able to effectively pin grain boundaries. The low solute content in these specimens before the annealing implies weaker pinning effect on polygonizing dislocations by concurrent precipitation as compared to specimens H1 and L1. The grains in the specimens H21, H31, L21 and L31 (homogenized at 450 °C) are coarser than in H1 and L1 but finer than in the specimens homogenized at 550 °C. The difference is again due to the impact of precipitates with different size and population with regard to pinning (Fig. 3). In both cases, the high-Mn specimens exhibit finer grains than the low-Mn specimens that might be attributed to the effect of Mn precipitation in the former ones.

The most significant factor that has affected the grain size in the investigated materials is the pre-strain. The effect of Mn solute supersaturation and concurrent precipitation on the grain size is less important, however, it cannot be neglected. On the other hand, the effect of Mn solute content on the texture is significant (see below).

The present investigation also indicates that cold rolling prior to homogenization significantly improves grain size uniformity (compare Fig. 4c,d with Fig. 4e, f). The improvement of grain size uniformity by cold rolling might be accounted for by the uniformly distributed dislocations in the entire specimen volume introduced by rolling. These dislocations promote the diffusion of solutes and serve as precipitation nucleation sites. As a uniform space distribution of pinning precipitates is created, the new grains formed during recrystallization are also uniform in size.

#### 4.3. Effect of Mn content on the texture

Our former [11, 16] and present results indicate that Mn in Al-Mg TRC alloys has a very prominent role in retarding recrystallization. The results indicate that Mn in solid solution also affects the texture. All specimens with high Mn content exhibit much weaker texture than the specimens with very low Mn content. Especially the strength of cube texture is significantly reduced by the presence of Mn.

These results are in agreement with the results of the investigations of Al-Mn alloys by Morris and Liu [10]. These authors reported that the recrystallization texture of a continuous-cast AA3015 alloy (Al-Mn-Mg alloy with up to 0.9 wt.% Mn) is characterized by a strong P orientation accompanied by a minor R-cube orientation when concurrent precipitation occurs. Both P and R orientations are observed in specimen H1 (Fig. 5a,c,d). Hence, as in Al-Mn-Mg alloys [10], the changed recrystallization mechanism (due to Mn precipitation) does not yield the strong cube texture normally found in the recrystallization texture of face-centered-cube (fcc) materials. The P component is formed during recrystallization and is stronger in intensity the greater the degree of cold rolling prior to the annealing is. The P orientation develops at the expense of the brass orientation  $\{110\} \langle 112 \rangle$  [10]. The development of the P component during annealing promoted by a concurrent precipitation is amplified by the decrease in stacking fault energy (SFE) due to the high solute supersaturation present in TRC alloys in contrast to DCC alloys. Therefore, the mechanism of cube texture weakening is probably linked with the presence of Mn solute and its effect on the development of P component and on the suppression of the development of cube component. This effect of Mn solute is not weak despite of the fact that the amount of Mn present in specimens H is relatively low.

Cube-oriented grains have special deformation properties and for this reason cold rolled Al alloy sheets contain cube-oriented subgrains with size exceeding the critical size for recrystallization nucleation [17]. Upon annealing, the cube subgrains can start growing without any incubation time while other sites

need an initial recovery period in order to achieve the critical size. However, the annealing regime used in this investigation involved a slow heating part, during which significant recovery and growth of subgrains of all orientations is expected. The solute atoms and precipitates present in the deformed matrix are expected to hinder the moving boundaries of all grains irrespective of grain orientation.

The effect of Mn solute atoms and/or Mn-precipitates on the modification of the texture is thus similar to the effect of Fe atoms in AlMg alloys investigated by Koizumi et al. in [6]. The impact of Mn solutes and precipitates consists of preventing cube nuclei growth. Solute atoms segregate on the boundaries of the early appeared cube subgrains and hinder them, i.e., prevent them from growing up to the critical size for grain nucleation [6]. The hindering effect of Mn-precipitates (forming concurrently with or prior to recrystallization) on the boundaries of cube nuclei during the early stages of recrystallization is thus an additional cause of the significantly lower strength of cube components in the alloys with high Mn content. In the specimens with low Mn content, the growth selection criterion [17] plays an important role because the growth of non-hindered cube subgrains and grains at the expense of other orientation can start at the very early stages of recrystallization. The less dense small precipitates in specimens Lxy (Fig. 3b) are not sufficiently effective in hindering subgrain boundaries.

As already mentioned above, precipitation occurring concurrently with recrystallization shifts its start and end to high temperatures. However, recrystallization at high temperatures usually occurs by the discontinuous mechanisms, for example by PSN and nucleation on HAGB. Therefore, in specimens with high solute content, the role of PSN producing randomly oriented nuclei [15] increases and the texture developed is weaker, like in the non-homogenized specimens. In the homogenized specimens with low solute content the recrystallization occurs at low temperatures and continuous recrystallization is the dominant mechanism. In continuous recrystallization, the nuclei grow only in the deformed parent grains and thus, the retained rolling component, i.e., the  $\beta$ -fibre, is stronger than in the non-homogenized specimens (Fig. 7). The  $\beta$ -fibre exhibits stronger S and Cu components and weaker brass component.

When no drag on cube nuclei boundaries by solute atoms or precipitates is present, a strong cube texture develops due to the growth advantage of cube orientations at the expense of other orientations, especially in specimens with low Mn content.

An additional effect on texture is linked with alloy chemistry. As mentioned above, PSN randomizes the texture. Since the fraction of eutectic clusters and colonies of constituent particles in the specimens H is higher, the role of PSN in these specimens is probably

more important as compared to specimens L. Therefore, the specimens with higher Mn and Mg content have more particles and clusters at which nucleate randomly oriented grains. This can result in an additional decrease of the strength of texture.

The contribution to texture randomizing by PSN is stronger in the mid-thickness of the specimens since the coarse particles are relatively more frequent here. The effect of PSN on the difference in texture between surface and mid-thickness is more pronounced in the specimens with low Mn content probably due to the fact that in these specimens the impact of concurrent precipitation is much smaller.

The weakening of the cube and the presence of P component in the specimens with Mn due to solute and precipitation concurrent to recrystallization alters the anisotropy of recrystallized sheets. The effect is due to the decrease in the intensity of  $0^\circ/90^\circ$  earing connected with the cube texture and to the low  $45^\circ$  earing induced by the P component.

#### 4.4. Effect of deformation degree prior to annealing on texture

The intensity of precipitation is affected by both solute content and dislocation density because the dislocations increase the mobility of Mn atoms and act as nucleation sites. Dislocations are introduced by cold rolling and their density usually increases with increasing degree of cold working. Furthermore, the start of recrystallization is shifted to lower temperatures by an increased degree of deformation. Therefore, the effect of solute atoms and precipitates on the recrystallization in the specimens with high deformation degree is strong. High deformation and high solute content are characteristic for the non-homogenized specimens and the impact of precipitation on the nucleation stage of recrystallization is the strongest. The concurrent precipitation exerts in this case the highest hindering effect on cube texture components and also contributes to the growth of P components at the expense of the brass components. The strong texture of the surface layers in specimen L1 (Fig. 6b) comprises strong rotated  $\text{cube}_{\text{ND}}$ ,  $\text{cube}_{\text{RD}}$  and  $\text{cube}_{\text{share}}$  components, in accordance with the results reported for a TRC AlFeSi alloy in [17].

## 5. Conclusions

The effect on Mn content and pre-treatment parameters on the grain structure and texture developed during industrial-like annealing of twin-roll cast AlMg3 alloys was investigated. The most significant factor affecting grain size and uniformity is the degree of deformation prior to annealing. The influence of Mn solute content and concurrent precipita-

tion on grain size is less pronounced but both solute content and precipitation reduce the strength of texture significantly. The most reduced texture component is the cube component but the components of the retained rolling texture are also weakened. The mechanisms of texture changes due to the presence of Mn solute and precipitation concurrent to recrystallization were elucidated. The high supersaturation of Mn in the solid solution of these materials ensures effective suppression of cube texture development and prevents the anisotropic behaviour in forming procedures. It was demonstrated that the technology based on TRC and a processing without homogenization of AA5754 alloys containing enough Mn is a cost effective and environment-friendly process for manufacturing automotive sheets with high strength and good formability.

## Acknowledgements

ASSAN Aluminium Works (Turkey) is acknowledged for supplying the input material. The financial support of the Czech Science Foundation in the framework of project No 106/05/2574 is gratefully acknowledged. Thanks are also due to Dr. J. Marek, CTU Prague, for carrying out the X-ray texture measurements.

## References

- [1] SUZUKI, M.: In: Mater. Sci. Forum. Vols. 519–521. Eds.: Poole, W. J., Wells, M. A., Lloyd, D. J. Uetikon-Zuerich, Trans Tech Publications Ltd. 2006, p. 11.
- [2] SLAMOVA, M.—OCENASEK, V.—CIESLAR, M.—CHALUPA, B.—MERLE, P.: In: Mater. Sci. Forum. Vols. 331–337. Eds.: Starke, E. A. Jr., Sanders, T. H. Jr., Cassada, W. A. Uetikon-Zuerich, Trans Tech Publications Ltd. 2000, p. 829.
- [3] BIROL, Y.—KARA, G.—DUNDAR, M.—CAKIR, O.—ZEYBEKOGLU, G.—AKKURT, S.—YILDIZ-BAYRAK, G.—ROMANOWSKI, C.: In: Proc. TMS Annual Meeting. Eds.: Das, S., Kaufman, G., Green, J. Warrendale, The Minerals, Metals & Materials Society 2001, p. 107.
- [4] LAHAYE, C. et al.: SAE Technical Paper series 1999-01-3173, 1999.
- [5] KOIZUMI, M.—KOHARA, S.—INAGAKI, H.: Z. Metallkd., 91, 2000, p. 460.
- [6] KOIZUMI, M.—SAITOU, T.—OKUDAIRA, H.—INAGAKI H.: Z. Metallkd., 91, 2000, p. 717.
- [7] COURT, S. A.—GATENBY, K. M.—LLOYD, D. J.: Mater. Sci. Eng., A319–A321, 2001, p. 443.
- [8] LUKÁČ, P.—KOCICH, R.—GREGER, M.—PADALKA, O.—SZÁRAZ, Z.: Kovove Mater., 45, 2007, p. 115.
- [9] CHENG, X.-M.—MORRIS, J. G.: Mater. Sci. Eng., A323, 2002, p. 32.
- [10] MORRIS, J. G.—LIU, W. C.: JOM, 2005, p. 44.
- [11] SLÁMOVÁ, M.—BIROL, Y.—HOMOLA, P.—SLÁMA, P.: In: Proc. IX Int. Conf. Aluminium in Transport 2003. Centre of Competence Central, Kraków, Institute of Non-Ferrous Metals 2003, p. 183.

- [12] BIROL, Y.: *Mat. Sci. and Techn.*, 22, 2006, p. 1.
- [13] BUNGE, H. J.: *Mathematical Methods of Texture Analysis*. London, Butterworth-Heinemann Ltd. 1984.
- [14] KARLÍK, M.—SLÁMOVÁ, M.—JANEČEK, M.—HOMOLA, P.: *Kovove Mater.*, 40, 2002, p. 330.
- [15] HUMPHREYS, F. J.—HATHERLEY, M.: *Recrystallization and Related Annealing Phenomena*. Oxford, Pergamon Press 1995.
- [16] SLÁMOVÁ, M.—SLÁMA, P.—HOMOLA, P.—KARLÍK, M.: In: *Mater. Sci. Forum*. Vol. 482. Ed.: Pokluda, J. Zürich, Trans Tech Publications Ltd. 2005, p. 279.
- [17] BENUM, S.—NES, E.: *Acta Mater.*, 45, 1997, p. 4593.